Nonlinear optical response of superlattices: Multistability and soliton trains

L. Kahn,* N. S. Almeida,† and D. L. Mills
Department of Physics, University of California, Irvine, California 92717
(Received 24 September 1987)

For models of finite superlattices, we calculate the power dependence of the transmissivity, when one film in each unit cell exhibits a nonlinear response to the electromagnetic field. We assume the nonlinearity has its origin in the spins in an antiferromagnetic film, illuminated with frequency near resonance; one then has a term in the magnetic susceptibility proportional to the local field intensity. Results very similar to ours follow for the case where the nonlinearity occurs in the dielectric response. The response is dependent on whether the frequency of the radiation lies within a stop gap of the dispersion relation of the infinite structure calculated in linear theory, or within our allowed band of propagating waves. In the former case, we find soliton trains and multistability, as discussed earlier by Chen and Mills. In the latter, we have multistability and transmissivity gaps similar to those reported earlier by Delyon *et al.* The method used presently is adapted from that employed by Delyon and co-workers; we discuss its relation to alternate computational approaches.

I. INTRODUCTION

Superlattice structures of impressive quality are now synthesized from films composed of a wide variety of materials. The earlier work placed primary focus on combinations of semiconducting materials such as GaAs and $Ga_xAl_{1-x}As$. More recently, we see structures which incorporate a variety of metallic films, including the ferromagnets Fe, Ni, and Gd, along with the spiral spin material Dy. Very-high-quality films of the antiferromagnet FeF_2 have been fabricated,[1] and we may expect these to be incorporated in superlattice multilayer structures in the near future.

Superlattice structures form a new class of artificial materials whose properties can be designed in advance, and in fact some of these may be unique to the multilayer structure. For example, we may have collective excitations such as plasmons[2] or spin waves[3] which are coherent modes which extend throughout the multilayer medium. It follows that the dispersion relation of these modes, and even the existence[3] of certain branches, is sensitive to the geometrical parameters of the superlattices. Through use of Brillouin scattering spectroscopy, spin-wave excitations in superlattices have been studied in a particularly quantitative manner,[4] to the point where information on the magnetization in the films may be extracted from the data.

Knowledge of the spectrum of elementary excitation spectrum of a superlattice allows one to describe its linear response to an external probe, such as an electromagnetic wave. The analysis can proceed in a manner familiar in the theory of solids.

In the recent theoretical literature, there has been discussion of the nonlinear optical response of superlattice structures, with emphasis on materials where the length of the unit cell is comparable to, or longer than, the wavelength of radiation in the material. In this regime, in linear theory, the superlattice may be viewed as a physical realization of the classic Kronig-Penney model discussed in introductory texts on solid-state theory.[5] The propagation of waves down the structure is described by a dispersion relation which contains gaps, here called stop gaps, at the Brillouin-zone boundary and center. Outside the stop gaps, one has the allowed bands where waves may propagate down the structure, with dispersion relation controlled by the solution of the appropriate Kronig-Penney description of the structure.

Chen and one of the present authors[6] have studied the nonlinear optical response of such a structure when it is illuminated by radiation with frequency in a stop gap. The source of the nonlinearity is a power dependence of the dielectric constant in one of the two films in the basic unit cell. These authors found that at rather low incident power, bistability (and, in fact, multistability) occurs with physical origin in solitons excited by the incoming electromagnetic wave. Subsequent papers have elaborated on this work.[7,8]

Delyon and co-workers[9] explored the power dependence of the transmissivity of a finite superlattice illuminated with radiation with frequency within an allowed frequency band. They also found bistability, and multistability. In addition, they find power ranges within which the superlattice becomes perfectly reflecting, in the sense that the field at the output end of a finite structure is smaller than that at the input end, by an amount $\exp(-\alpha L)$, with L the length of the superlattice.

The two sets of theoretical studies show that the nonlinear-response characteristics of superlattices are rich in properties, and unique to these periodic structures. It is, unfortunately, difficult to make direct comparisons between the results of Chen and Mills, who explored the nonlinear response only for frequencies within a stop gap, and the results of Delyon *et al.*, who examined only frequencies within an allowed band. The underlying model superlattices are different in each case, and the results are presented in a sufficiently different

manner that a direct comparison is very difficult. For example, one would like to inquire if the gap-soliton-mediated bistability discussed by Chen and Mills occurs at power levels substantially lower than, or substantially higher than, the transmission anomalies discussed by Delyon *et al.* Furthermore, the two sets of authors have employed very different theoretical methods to address the questions.

It would therefore be most helpful, in our view, to see a comprehensive study of both sets of nonlinear anomalies for the same model superlattice, and within the same theoretical framework. The purpose of this paper is to present such a study. We also present a number of new results, not found in either of the previous studies. For frequencies within the allowed band, we show the spatial variation of the field intensities within the superlattice structure. These provide insight into the physical origin of the nonlinear anomalies. For frequencies within a stop gap, we extend the earlier calculations of Chen and Mills to much higher power levels, where we find marked differences in the nature of the instabilities.

We make a specific choice of the model superlattice, in our analysis, so quantitative numerical results are presented for a well-defined physical system. The model is a superlattice constructed of alternating layers of dielectric, and an (insulating) antiferromagnetic film, assumed to be placed in zero external magnetic field. Thin films of FeF_2 have been fabricated recently with very narrow resonances[1] in the far infrared, and our recent theoretical analysis[10] shows that when such films are illuminated with radiation very close to the antiferromagnetic resonance frequency, their nonlinear response to an electromagnetic wave is very large, by virtue of nonlinearities in the magnetic permeability. While structures of the sort explored here have yet to be synthesized, and in this sense our model superlattice is academic in nature, it is possible in principle to fabricate such a multilayer structure. The principal aim of this work is to discuss the two very different classes of nonlinear behavior explored earlier within a single model calculation, so we do not regard this as a serious problem.

It is our view that magnetic materials, and most particularly high-quality single films of such materials as FeF_2, offer exciting possibilities for the future, as nonlinear (tunable) elements for the far-infrared frequency range.

The nonlinear instabilities explored here require structures whose unit-cell dimensions are comparable to a wavelength of the modes which propagate in the structure. This is quite clear for the gap soliton mediated bistability, since to operate within a stop gap, one must employ radiation whose wavelength is on the scale of the unit cell. At visible or infrared frequencies, this means the structures appropriate for such studies will consist of films very much thicker than those incorporated into many of the semiconducting or metallic superlattices discussed in the current literature. It should be the case also that the demands on interface quality will not be particularly high, i.e., one will not require perfection on the atomic scale, so far as we can see. This suggests the experimentalists should be able to synthesize appropriate structures from a variety of materials.

II. FORMALISM

We consider a plane-polarized electromagnetic wave propagating normal to the interfaces of the superlattice. The antiferromagnet is assumed to be an easy-axis, two-sublattice material with easy axis normal to the interfaces. If no external magnetic field is present, then the plane-polarized wave propagates through the medium with no rotation of the plane of polarization. This remains true in the presence of nonlinear contributions to the magnetic susceptibility tensor.[10] We then may write down the wave equation obeyed by the single Cartesian component of magnetic field, $h(z,t)=h(z)\exp(-i\Omega t)$. In the antiferromagnet as described above, with lowest-order nonlinearity included, we have

$$\frac{d^2h}{dz^2}+k^2[1+4\pi\chi(1+\lambda\,|\,h\,|^2)]h=0\ , \tag{2.1}$$

where $k^2=\Omega^2\epsilon_\perp/c^2$, with $\epsilon_\perp$ the dielectric constant in the basal plane. In Eq. (2.1), χ is the linear magnetic susceptibility of the material, and λ describes the lowest-order nonlinearity. If Ω_0 is the antiferromagnetic resonance frequency in zero magnetic field, M_s the magnetization of one sublattice, H_A the strength of the anisotropy field, and γ the gyromagnetic ratio, we have[10]

$$\chi(\Omega)=\frac{2\gamma^2H_AM_s}{\Omega_0^2-\Omega^2}\ , \tag{2.2a}$$

and the parameter λ in Eq. (2.1) is frequency dependent, given by the expression[10]

$$\lambda(\Omega)=\frac{3}{2}\frac{\gamma^2\Omega^2(\Omega^2+\gamma^2H_A^2)}{(\Omega_0^2-\Omega^2)^3}\ . \tag{2.2b}$$

The nonmagnetic film is described by setting $\chi=0$, and replacing $\epsilon_\perp$ by the appropriate dielectric constant ϵ_0. Boundary conditions are that h be continuous at each interface, along with the product $(dh/dz)\epsilon^{-1}$, with ϵ the dielectric constant in the appropriate material.

Earlier papers[6–9] explored model dielectric superlattices, in which the magnetic permeability is unity everywhere, and the nonlinearity resides in the dielectric response. The present set of equations and boundary conditions can be mapped onto those used earlier by replacing $h(z)$ by $\psi(z)=h(z)/\epsilon$ everywhere, where ϵ is the appropriate dielectric constant. Thus, the conclusions we reach are directly applicable to dielectric superlattices, save for the quantitative aspects.

We could proceed to study the solutions of the above set of equations by expressing their solutions in terms of elliptic integrals (in the nonlinear film), then employing the identities developed by Chen and Mills[8] to eliminate all but one parameter, the transmissivity. Instead, we choose here to follow Delyon and co-workers, who proceed by a direct real-space integration, introducing a grid of points z_n. If ϵ is the dielectric constant outside the finite superlattice structure ($\epsilon=1$ for vacuum), we begin by writing Eq. (2.1) in the form, with $k_0^2=\Omega^2\epsilon/c^2$,

$$\frac{d^2h}{dz^2}+k_0^2h=k_0^2\left[1-\frac{\epsilon_\perp}{\epsilon}(1+4\pi\chi+4\pi\chi\lambda\,|\,h\,|^2)\right]h\ , \tag{2.3}$$

where it is understood that the terms on the right-hand side are nonzero only within the sample. Then if h_i is the incident field, we let $\phi_n=h(z_n)/h_i$, and case Eq. (2.3) in the form

$$E\phi_n+\phi_{n+1}+\phi_{n-1}=(\alpha_0-\alpha_1\,|\,h_i\,|^2\,|\,\phi_n\,|^2)\phi_n\ , \tag{2.4}$$

where $E=-2+K^2$, and $K=k_0\xi$, with ξ the width of the interval in the basic spatial grid. We have $\alpha_0=K^2[1-(1+4\pi\chi)(\epsilon_\perp/\epsilon)]$ and $\alpha_1=K^2 4\pi\chi\epsilon_\perp\lambda/\epsilon$. We notice that the nonlinear term on the right-hand side of Eq. (2.4) exists only within the magnetic film, and $\alpha_0=K^2[1-(\epsilon_0/\epsilon)]$ within the dielectric layers.

Let the grid be chosen so that z_n with $0\le n\le N$ covers the space occupied by the finite superlattice. The superlattice is illuminated by a wave incident from the left, in the region where $n\le 0$. Then to the right we have only the transmitted wave. Thus, we have

$$\phi_n=\begin{cases}\exp(iKn)+R\exp(-iKn+i\zeta), & n\le 0 \quad (2.5a)\\ T\exp(iKn), & n\ge N \quad (2.5b)\end{cases}$$

where in Eq. (2.5a) R is a real number. Our aim is to calculate the transmission coefficient T.

We now let $\psi_n=\phi_n/|\,T\,|$, and rearrange Eq. (2.4),

$$\psi_{n-1}=-\psi_{n+1}-(E-\alpha_0+\alpha_1\,|\,h_i\,|^2\,|\,T\,|^2\,|\,\psi_n\,|^2)\psi_n\ , \tag{2.6}$$

where now the asymptotic forms are

$$\psi_n=\begin{cases}R_0e^{iKn}+R_1e^{-iKn_e i\zeta}, & n\le 0 \quad (2.7a)\\ e^{iKn}, & n\ge N \quad (2.7b)\end{cases}$$

where $R_0=1/|\,T\,|$ and $R_1=R/|\,T\,|$.

There are conservation laws contained in the above finite-difference equations. Let the three points $n-1$, n, and $n+1$ lie within one medium. We then have the identity, which follows from Eq. (2.6),

$$\psi_n^*\psi_{n+1}-\psi_n\psi_{n+1}^*=\psi_{n-1}^*\psi_n-\psi_{n-1}\psi_n^*\ , \tag{2.8}$$

which means that within each film the quantity

$$J_n=\psi_n^*\psi_{n+1}-\psi_n\psi_{n+1}^* \tag{2.9}$$

is conserved.

Our boundary conditions are that ψ_n is continuous across each boundary (conservation of tangential h), and also $(1/\epsilon)(dh/dz)$ is continuous across each boundary (conservation of tangential electric field). Let points $(n-1,n)$ lie in medium 1, and points $n+1$, $n+2$ lie in medium 2. The boundary conditions then translate into the requirement

$$\psi_n=\psi_{n+1}\ , \tag{2.10a}$$

and

$$\frac{1}{\epsilon_1}(\psi_n-\psi_{n-1})=\frac{1}{\epsilon_2}(\psi_{n+1}-\psi_{n+2})\ , \tag{2.10b}$$

which after a few lines of algebra can be translated into the requirement

$$\frac{1}{\epsilon_1}J_{n-1}=\frac{1}{\epsilon_2}J_{n+1}\ , \tag{2.11}$$

i.e., the quantity J_n/ϵ_i is conserved at each interface. The time average of the Poynting vector for our problem is

$$\langle S\rangle=\frac{c^2}{16\pi\Omega\epsilon_i i}\left[h^*\frac{dh}{dz}-h\frac{dh^*}{dz}\right]$$
$$=\frac{c^2\xi}{16\pi\Omega\epsilon_i i}(h_n^*h_{n+1}-h_nh_{n+1}^*)\ , \tag{2.12}$$

so the condition in Eq. (2.11) is equivalent to the requirement that the energy per unit time flowing down the structure is independent of z, as it should be.

We then let

$$\frac{1}{\epsilon_i}(\psi_n^*\psi_{n+1}-\psi_n\psi_{n+1}^*)=A\ , \tag{2.13}$$

with A a constant, where on the left-hand side the dielectric constant of the medium within which the points $(n,n+1)$ lie is to be inserted.

Assuming for $n\ge N$ we have a medium with dielectric constant ϵ,

$$A=\frac{1}{\epsilon}(e^{iK}-e^{-iK})=\frac{2i}{\epsilon}\sin(K)\ , \tag{2.14}$$

so that

$$\psi_n^*\psi_{n+1}-\psi_{n+1}^*\psi_n=2i\frac{\epsilon_i}{\epsilon}\sin(K)\ . \tag{2.15}$$

By exploiting the conservation law just described, we may simplify the task of solving the finite-difference equation. Let $F(|\,\psi_n\,|^2)=E-\alpha_0+\alpha_1|\,h_i\,|^2|\,T\,|^2|\,\psi_n\,|^2$. From Eq. (2.6), one may derive the relation

$$|\,\psi_{n-1}\,|^2=|\,\psi_{n+1}\,|^2+[F(|\,\psi_n\,|^2)]^2\,|\,\psi_n\,|^2$$
$$+F(|\,\psi_n\,|^2)(\psi_n^*\psi_{n+1}+\psi_n\psi_{n+1}^*)\ , \tag{2.16}$$

while multiplying each side of Eq. (2.15) by its complex conjugate gives

$$\psi_n^2(\psi_{n+1}^*)^2+(\psi_n^*)^2(\psi_{n+1})^2$$
$$=2\left[|\,\psi_n\,|^2\,|\,\psi_{n+1}\,|^2-2\frac{\epsilon_i^2}{\epsilon^2}\sin^2(K)\right]\ , \tag{2.17}$$

so we have

$$|\psi_{n-1}|^2=|\psi_{n+1}|^2+[F(|\psi_n|^2)]^2|\psi_n|^2 +2\left[|\psi_n|^2|\psi_{n+1}|^2-\frac{\epsilon_i^2}{\epsilon^2}\sin^2(K)\right]^{1/2} \times F(|\psi_n|^2) . \quad (2.18)$$

This result is very similar to the principal result of Ref. 9, except the square root is missing from the third term in the equation displayed in their text (we assume this error to be of typographical origin). When Eq. (2.18) is applied to the antiferromagnet, we have seen that $\epsilon_i=\epsilon_\perp$, with $F=E-\alpha_0+\alpha_1|h_i|^2|T|^2|\psi_n|^2$, while for the nonmagnetic film, $\epsilon_i=\epsilon_0$ and $F=E-\alpha_0$ only.

The virtue of Eq. (2.18) is that it involves the real number $|\psi_n|^2$ only. Once we know $|\psi_n|^2$ and $|\psi_{n+1}|^2$, we can calculate $|\psi_{n-1}|^2$, and thus iterate from right to left beginning on the output side of the superlattice.

In Ref. 9, $|\psi_n|^2$ was denoted by x, $|\psi_{n+1}|^2$ as y, and $|\psi_{n-1}|^2$ by x', so if we use this notation, Eq. (2.18) becomes

$$x'=y+F^2x+2\left[xy-\frac{\epsilon_i^2}{\epsilon^2}\sin^2(K)\right]^{1/2}F , \quad (2.19)$$

where $F=E-\alpha_0-\alpha_1|h_i|^2|T|^2x$. Conservation of $h(z)$ at each boundary, combined with conservation of $(1/\epsilon)(dh/dz)$ means that at each boundary, we have

$$\lim_{\delta\to 0}\frac{1}{\epsilon_-}\frac{d}{dz}|h|^2 z_0-\delta=\lim_{\delta\to 0}\frac{1}{\epsilon_+}\frac{d}{dz}|h|^2 z_0+\delta . \quad (2.20)$$

If now we work with a grid which places point n precisely on the boundary between the two media, we have

$$\frac{1}{\epsilon_-}(x'-x)=\frac{1}{\epsilon_+}(x-y) . \quad (2.21)$$

Equations (2.19) and (2.21) represent the formal results that provide the basis for our analysis. We next turn to a description of how this mathematical method is applied, and illustrate how the results of an earlier paper, which used a rather different approach, may be recovered.[10]

III. RESULTS AND DISCUSSION

Before we examine superlattice structures, it will prove useful to consider a single, isolated film of FeF_2 modeled as discussed in Sec. II. The power dependence of the transmissivity of such a film was explored in Ref. 10, through use of a very different theoretical approach. Our first step is to establish contact between the two very different calculations. As we do this, we will obtain insight into useful features of the present method.

On the output side of the film (assumed to be vacuum), we have only the transmitted wave, which is necessarily a simple plane wave with amplitude $|T|$. Thus, we have $x=y=1$ here. The boundary condition at the interface [Eq. (2.21)] implies $x'=1$, i.e., continuity of the derivative of the intensity, which is zero outside the film. For convenience, and in fact as a matter of practical necessity, we introduce a new variable $h_0=h_i|T|$, since at this point we have no knowledge of the transmission coefficient $|T|$. It is h_0 we use as the parameter which, in the units of Sec. II, control the strength of the nonlinearity. For a given value of h_0, through use of Eq. (2.19), we may iterate through to the left-hand (input) side of the film, at which point Eq. (2.21) is applied again. This application of the boundary condition yields nontrivial results.

We now need to determine the value of $|T|$. This is accomplished through the following technique. The solution is continued to the left into the vacuum, and we see from Eq. (2.7) that it oscillates between the values $Z_{\max}=(R_0+R_1)^2$ and $Z_{\min}=(R_0-R_1)^2$. Since $|T|^2=1/|R_0|^2$, we arrive at

$$|T|^2=\frac{4}{(Z_{\min}^{1/2}+Z_{\max}^{1/2})^2} . \quad (3.1)$$

Note that the condition $R_0^2-R_1^2=1$ (energy conservation) implies that $Z_{\max}Z_{\min}=1$. This guarantees that $|T|^2\le 1$. The value of h_0 was used as input, and since $h_0=h_i|T|$, now that we know $|T|$, the value of the incident field h_i corresponding to $|T|$ is uniquely determined.

From this discussion, it is clear that for each choice of h_0 we determine a unique value of $|T|$. We may then see how bistability (or multistability) emerges from the analysis by consulting Fig. 1. In Fig. 1(a), we show $|T|$ as a function of the parameter h_0. The single-valued nature of the relationship between the two parameters is evident. We see oscillations in the transmissivity characteristic of a thin film whose index of refraction is varied through some external means; the transmissivity reaches unity whenever an integral number of half-wavelengths fits into the film. The analogy is not a precise one, of course, because in our case the change in effective index is not independent of position, but in fact varies with the local intensity of the wave. In Fig. 1(b), we plot the intensity of the transmissivity $|T|^2$ as a function not of h_0, but of the actual incident-field amplitude $h_i=h_0/|T|$. We see the characteristic signature of bistability in the response, once the information in Fig. 1(a) is rearranged into the form of a proper input-output plot. We have compared results obtained by the present method with those presented earlier,[10] and the two give identical results.

Our earlier studies of the nonlinear optical response of a thin film[10–13] and of multilayer structures expressed the solution to the basic differential equation, Eq. (2.1), in terms of Jacobi elliptic functions. These contain certain constants of integration in their arguments which make the task of satisfying the boundary conditions at each interface difficult to implement. A series of identities was derived that enabled one to express all constants in terms of the transmissivity $|T|$. A consistency relation was developed which, if satisfied for a given value of the incident field h_i and choice of $|T|$, ensured that one had a solution in hand. Then for a given choice of h_i, one had to search for all values of $|T|$ in the range $0\le|T|\le 1$ for which a solution can be achieved. In regions where

bistability occurs, one finds three values of $|T|$ for a given value of h_i, and there are more in regimes of multistability.

The method used in these earlier papers is very much easier to implement than approaches put forward by earlier authors.[14] At the same time, the method employed here, set forth first in Ref. 9, is simpler yet, in that the need to search for allowed values of $|T|$ is eliminated. Finally, the approach developed by Chen and Mills allowed one to explore rather large structures, with up to 120 unit cells. It proves difficult to maintain accuracy with a finite-difference method for a structure that large.

We should mention that the results obtained with the finite-difference approach converge quickly with decreasing ξ. In the example displayed in Fig. 1, where the slab thickness equals $\lambda_0/2$, with λ_0 the vacuum wavelength of the incident radiation, the choice $\xi=\lambda_0/2000$ proved more than adequate to give convergent results.

We now turn to multilayer systems, which we model as stacks of bilayers. Each bilayer consists of one dielectric film, and one film of FeF_2. The parameters representative of FeF_2 are $\epsilon_\perp=4$, the anisotropy field H_A is 200 kG, the exchange field H_E is 540 kG, while the saturation magnetization of one such lattice is 0.56 kG. We suppose the dielectric film is ZnF_2, which is diamagnetic, and for which $\epsilon_\perp=8$.[15] We examine these systems in two limits, (a) thick slabs, where each film in the bilayer has equal thickness, and the width d of each bilayer equals the vacuum wavelength λ_0, and (b) thin slabs, where $d=\lambda_0/10$.

To assist in interpreting the results, and to guide the calculation of the nonlinear response, we begin by calculating the dispersion relation for propagation of electromagnetic waves in the structure, in the direction normal to the interface, in linear theory. With the nonlinear terms set to zero, the model system is a physical realization of the classical one-dimensional Kronig-Penney model. The normal modes have the character of Bloch waves of wave vector Q, and the associated dispersion relation has stop gaps at the various Brillouin-zone boundaries. If $\mu=1+4\pi\chi_0$, and d_1 and d_2 are the thicknesses of the two films in the basic bilayer, the dispersion relation for such a structure is found from the roots of

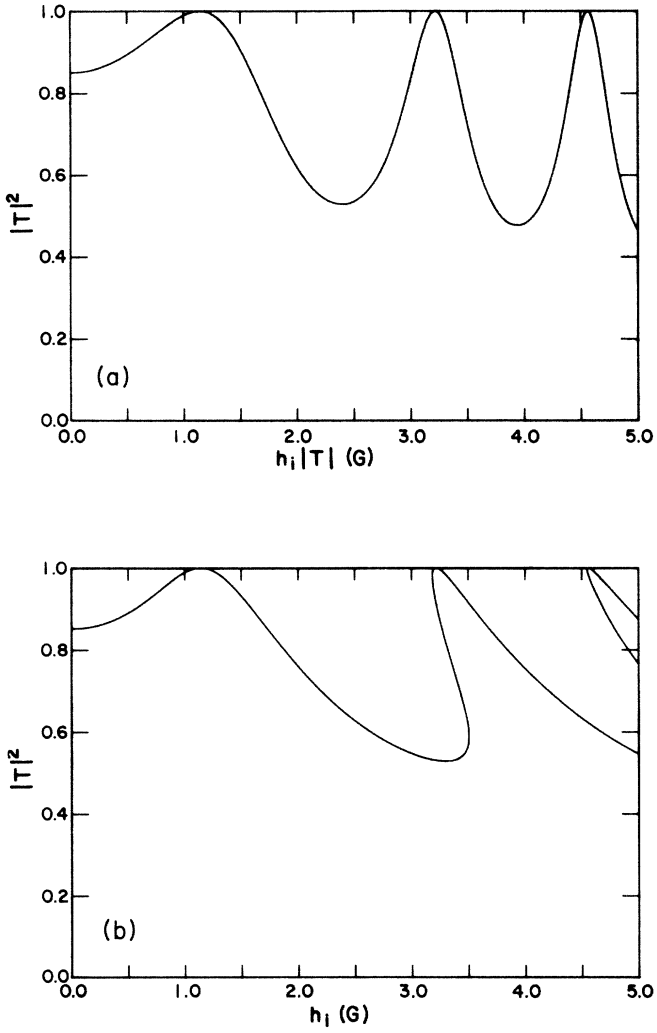

FIG. 1. (a) A plot of $|T|^2$ as a function of $h_i|T|$ for a single film of FeF_2 with thickness $d_1=\lambda_0/2\cong 105$ μm, and for a frequency $(\Omega-\Omega_0)/\gamma$ of 150 G (i.e., a frequency 150 G above the antiferromagnetic resonance frequency). The units of h_i are G. (b) The same as (a), but now we plot $|T|^2$ as a function of h_i.

$$\cos Q(d_1+d_2)=\cos\left[\frac{\omega}{c}d_1(\epsilon_1\mu_1)^{1/2}\right]\cos\left[\frac{\omega}{c}d_2(\epsilon_2\mu_2)^{1/2}\right]-\frac{1}{2}\left[\left[\frac{\epsilon_1\mu_2}{\epsilon_2\mu_1}\right]^{1/2}+\left[\frac{\epsilon_2\mu_1}{\epsilon_1\mu_2}\right]^{1/2}\right]\sin\left[\frac{\omega}{c}d_1(\epsilon_1\mu_1)^{1/2}\right]\sin\left[\frac{\omega}{c}d_2(\epsilon_2\mu_2)^{1/2}\right]. \tag{3.2}$$

When the right-hand side of Eq. (3.2) is less than unity, the frequency ω lies within an allowed band, while when it has magnitude greater than unity we are within a stop gap. The wave vector Q always lies within the first Brillouin zone of the structure, $-\pi(d_1+d_2)\leq Q\leq+\pi/(d_1+d_2)$. In Fig. 2(a), we show the dispersion relation of several bands in the structure with $d_1=d_2=\lambda_0/2$; recall that Ω_0 is the antiferromagnetic resonance frequency, and we measure $(\Omega-\Omega_0)$ in G. In Fig. 2(b), we show the transmissivity $|T|^2$ as a function of frequency, for eight bilayers, calculated within linear theory. The influence of the stop bands is evident, and within the allowed bands, the oscillatory structure has its origin in the standing-wave resonances of the finite structure. The "noise spikes" within the stop gaps are evidence of numerical errors in the finite-difference method.

In Fig. 3(a), for $(\Omega-\Omega_0)/\gamma=150$ G, we plot $|T|^2$ as a function of the parameter $h_i|T|$ for two bilayers with $d_1=d_2=\lambda_0/2$. In this structure, and for this particular frequency, $|T|^2=1$ in the linear theory.

Two distinct regimes are evident in Fig. 3(a). We have a slow monotonic falloff in $|T|^2$ with $h_i|T|$ initially, and the curve plummets dramatically just above $h_i|T| \cong 0.6$. Then we have a series of oscillatory resonances that corresponds to nonlinear standing-wave resonances of the structure. We shall comment further on this point later.

In Fig. 3(b), we rearrange the information in Fig. 3(a), so we have a plot of the transmitted power $P_T=|T|^2 h_i^2$, as a function of incident power, $P_i=h_i^2$, where h_i is measured in G. In earlier papers, plots of $|T|^2$ as a function of incident power were presented. We now choose to present the information according to the scheme used in Fig. 3 of Ref. 9, so our results may be compared directly to those obtained by Delyon *et al.*

We see that at low powers P_T is linearly related to P_I, as required in linear theory. The curve of P_T versus P_I saturates, and we see the tail end of a reentrant feature, above $P_I \cong 3.3$. This is our first hint of the complex structures reported in Ref. 9. The remaining features in Fig. 3(a) map into the region far to the right in Fig. 3(b), and are not evident in the plot.

In Fig. 4, we plot the square of the field in the structure, for the frequency used in Fig. 3 and the two-bilayer system, and for $h_i|T|=1.03$, corresponding to the second small resonant peak in Fig. 4. We see the standing-wave character of the resonance. The first film on the right-hand side of the structure is an antiferromagnet, and we see eleven resonant peaks within this film, counting the peak at the surface. In the second antiferromagnetic film, evidently the field intensity is lower, and there are only nine peaks. We see here the role of the nonlinearity in the effective index of refraction. On the average, the effective index is smaller in the second film, and the average wavelength longer as a consequence. If we move to the next-higher resonance peak in Fig. 3(a),

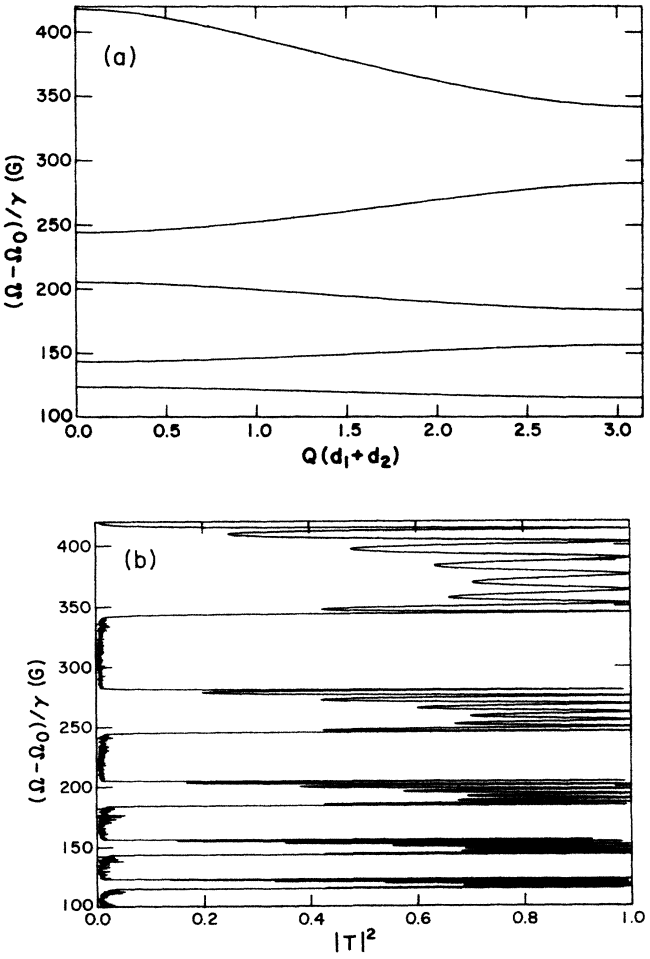

FIG. 2. (a) The dispersion relation for an infinite, linear model superlattice with alternating layers of antiferromagnetic (FeF_2) and dielectric (ZnF_2) materials, with thicknesses $d_1=d_2=\lambda_0/2$. (b) A plot of $|T|^2$ vs frequency, for eight bilayers, calculated in linear theory, for the same parameters used in (a).

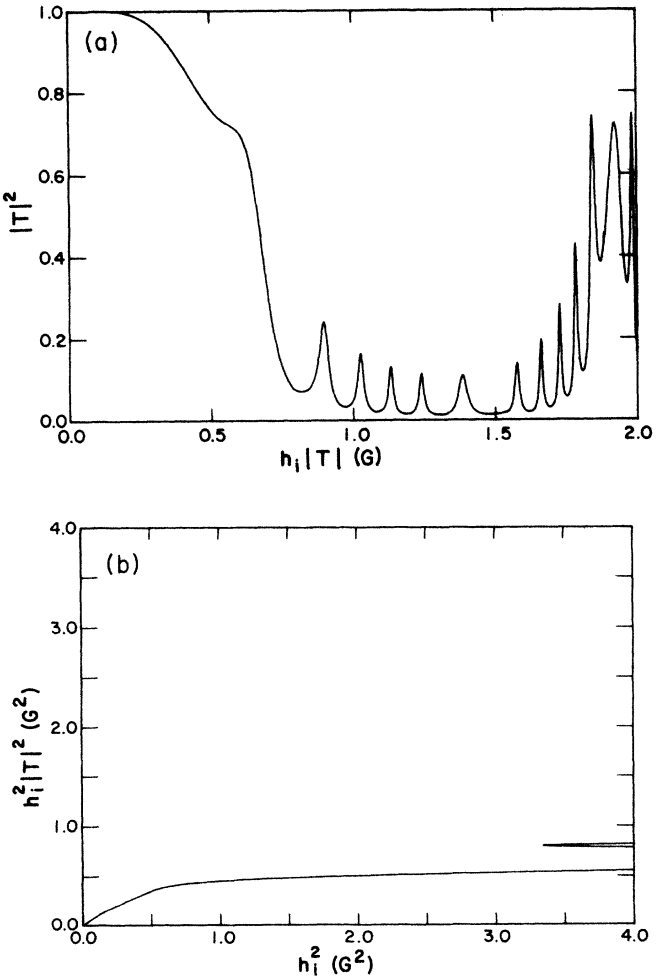

FIG. 3. (a) The transmissivity $|T|^2$, as a function of $h_i|T|$ for two bilayers, with $d_1=d_2=\lambda_0/2$. An antiferromagnetic film is exposed to the incident wave and we have $(\Omega-\Omega_0)/\gamma=150$ G. (b) The transmitted power $h_i^2|T|^2$, plotted as a function of $P_I=h_i^2$ for the same two-bilayer system considered in (a). Here the incident field is measured in G.

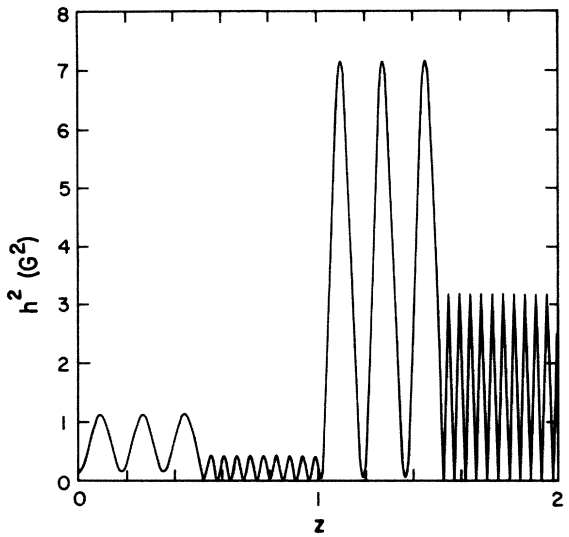

FIG. 4. For the two-bilayer structure explored in Fig. 3, and for $h_i \mid T \mid = 1.03$ corresponding to the second small resonance in Fig. 3(a), we plot the square of the field as a function of position. The incident wave is incident from the right, and the first film is an antiferromagnet, and distance is measured in units which makes the thickness of one bilayer equal unity.

we find exactly one more oscillation in the whole structure.

In Fig. 5(a), for a set of eight bilayers each identical to those used in Fig. 3(a), and again for $(\Omega-\Omega_0)/\gamma = 150$ G, we show a plot of $\mid T \mid^2$ versus the parameter $h_i \mid T \mid$. We again see smooth behavior below $h_i \mid T \mid \approx 0.6$, and then $\mid T \mid^2$ plummets rapidly. Beyond this apparent threshold, we see very fine oscillations in $\mid T \mid^2$. The figure has a chaotic appearance, but in fact these are finely spaced resonances, much narrower and much closer together than those in Fig. 3(a), beyond $h_i \mid T \mid \approx 0.6$. Figure 5(b) is a plot of the transmitted power, as a function of incident power, constructed by rearranging the information in Fig. 5(a). The figure reminds one of Fig. 3 in Ref. 9. Below $P_I \cong 0.5$ G^2, we have reentrant, and, consequently, bistable behavior, and above this value P_T is a complex, very multivalued function of P_I. Each of the fine features in the plot have finite widths, which do not show on the scale of the graph. We assume that an actual structure exposed to radiation so strong as to enter the multivalued regime will exhibit an apparently chaotic response to small changes in input power.

We have explored the response characteristics of three, four, five, and six bilayers identical to those used in Figs. 3 and 5, with $(\Omega-\Omega_0)/\gamma = 150$ G. In the plots of $\mid T \mid^2$ as a function of $h_i \mid T \mid$, we always find smooth behavior of $\mid T \mid^2$ in the region $h_i \mid T \mid \leq 0.6$, and $\mid T \mid^2$ drops off sharply at this value, to display a sequence of well-defined resonant peaks above this value of $h_i \mid T \mid$. To the eye, all the curves display the two distinct regions, and the transition from smooth behavior at small $h_i \mid T \mid$ to the regime with closely spaced resonance peaks at large values of this parameter is independent of the number of bilayers present. We do not understand the physical reason why this is so.

Beyond the "threshold" at $h_i \mid T \mid \cong 0.6$, examination of plots of the square of the field as a function of $h_i \mid T \mid$ leads one to understand the origin of the resonant peaks for $h_i \mid T \mid \gtrsim 0.6$. As discussed earlier for the two-bilayer case, these are nonlinear standing-wave resonances of the whole structure. As one moves from one resonance to the next, examinations of plots such as given in Fig. 4 show these to be just one more half-"wavelength" in the field pattern within the whole structure (not within one or each film). As the number of bilayers is increased, a smaller increment in the parameter $h_i \mid T \mid$ is thus required to move from one resonance to the next, and the pattern becomes progressively finer as bilayers are added until by the time we reach eight bilayers the plots provide an illusion of chaotic response. We should remark that for eight bilayers we have reduced ξ to $\lambda_0/20\,000$, and we have been careful to examine portions of the plot in sufficient detail to convince ourselves that the structure is real; it is too laborious to check every detail in the figure with such care, unfortunately.

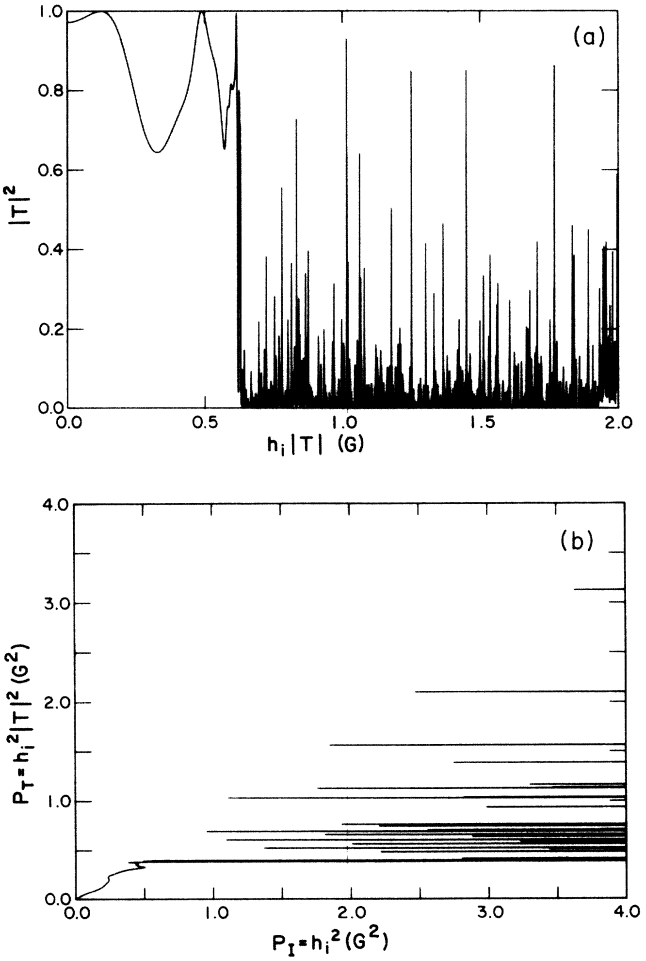

FIG. 5. (a) The same as Fig. 3(a), but now we have eight bilayers in the structure rather than two. (b) The same as Fig. 3(b), with eight bilayers.

We have also explored soliton trains excited by radiation with frequency inside one of the stop gaps of linear theory. Examination of earlier calculations,[6,8] along with an approximate analytic treatment shows that for frequencies near a gap edge, where classical sine-Gordon solitons are excited, the soliton envelope is quite broad, and extends over many unit cells. Since it is difficult to integrate the finite-difference equations over such a long distance and maintain accuracy, we turn our attention to a superlattice constructed of much thinner films, with thickness $\lambda_0/20$ rather than $\lambda_0/2$.

In Fig. 6, we show a plot of $|T|^2$ as a function of $h_i|T|$, for a superlattice composed of 20 bilayers; each film in the structure has the thickness $\lambda_0/20$. In linear theory, the structure has a wide stop gap which lies between $(\Omega-\Omega_0)/\gamma=127$ G and $(\Omega-\Omega_0)/\gamma=900$ G. The frequency used in the calculation is $(\Omega-\Omega_0)/\gamma=129$ G, and thus lies near the lower gap edge of linear theory. We see that the transmissivity is very small at low powers, as expected, and a series of dramatic transmission resonances in the range $0\leq h_i|T|\leq 0.6$ reminiscent of the soliton-mediated transmission resonances discussed earlier. Then just above $h_i|T|\cong 0.5$, once again we see a transition over to noisier behavior.

In Figs. 7(a) and 7(b), we plot the square of the field as a function of position in the 20-bilayer structure, and the first and second transmission resonances of Fig. 6. We see soliton trains reminiscent of the earlier work.[6,8] However, in the earlier studies, the first transmission resonance corresponded to a single solitonlike object in the structure, the second corresponded to two, and so on, while here, as just remarked, the first resonance corresponds to a pair, the second corresponds to three, and so on. Evidently, for the example chosen, a single soliton cannot be excited by the incoming field. The analytic description[7] of superlattice gap solitons, valid only in certain limits not applicable directly to the present example, provides us with a guide to the reasons for this. The size of the basic soliton varies inversely with the square root of the difference in the frequency of the incident wave, and the frequency of the nearby gap edge. In this example, the frequency is sufficiently far from the gap edge (farther, in reduced units, than used in the earlier calculations) that the basic soliton size is quite small compared to the length of the superlattices, and two must then be placed side by side before the amplitude- and slope-matching conditions can be met. We have tested this in two ways. First, if we decrease $(\Omega-\Omega_0)/\gamma$ from 129 to 127.5 G, much closer to the lower gap edge of 127 G, we find the one-soliton state as the lowest resonance. Secondly, if we double the size of the superlattice from 20 to 40 bilayers, with the frequency at the original 129 G, then the first resonance occurs at the same value of $h_i(T)$

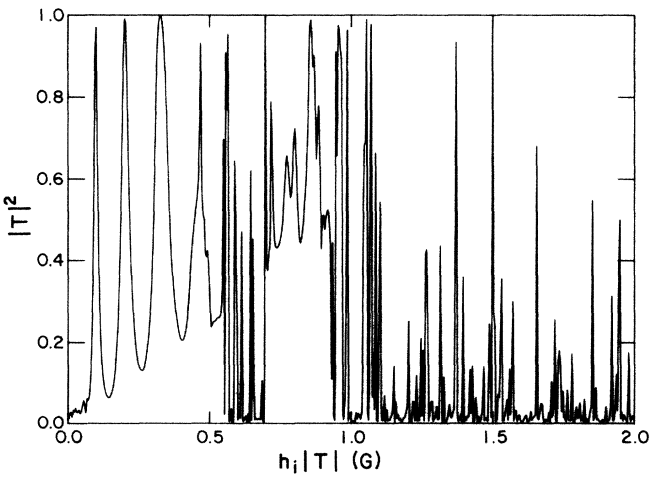

FIG. 6. For a superlattice constructed of 20 bilayers, each of total thickness $\lambda_0/10$ (thickness of each film $\lambda_0/20$), we show $|T|^2$ as a function of $h_i|T|$. In the structure, there is a wide stop gap that extends from $(\Omega-\Omega_0)\gamma$ of 127 to 900 G, and the frequency used, $(\Omega-\Omega_0)/\gamma=129$ G, lies near the lower gap edge.

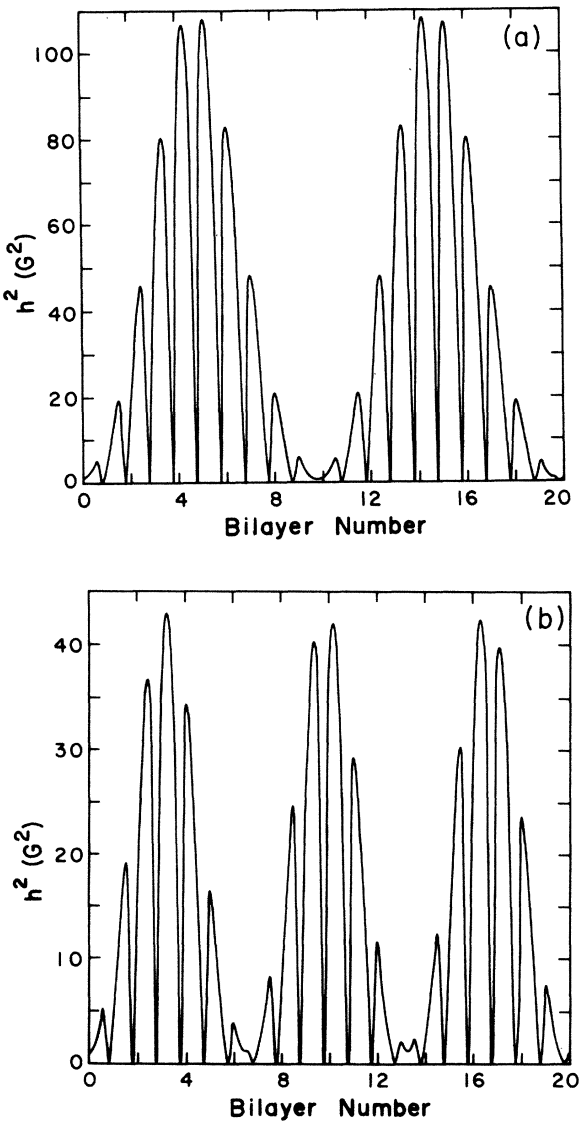

FIG. 7. A plot of the square of the field as a function of position in the 20-bilayer superlattice, for $h_i|T|$ set at (a) the first transmission resonance in Fig. 6, and (b) the second transmission resonance in Fig. 6. Distance units are such that the thickness of one bilayer is unity.

as for the 40-bilayer case. But then the first resonance is a four-soliton state, as illustrated in Fig. 8.

We should comment briefly on the terminology we have used in the discussion just given. The point is that the term "soliton" has been used in a rather imprecise manner. As pointed out earlier, for frequencies within a stop gap, the nonlinear wave equation applied to the periodic structure admits soliton solutions for the *infinitely long* superlattice. This was demonstrated numerically first for a dielectric superlattice,[6] and then in certain limits it may be demonstrated analytically that a double sine-Gordon equation is satisfied by a phase variable which characterizes the gap soliton.[7] These solitons are states in which the time-averaged energy flow normal to the interfaces is identically zero. Only single solitons emerge from the analysis, and not "soliton trains" such as those shown in Figs. 7 and 8.

Consider, for simplicity, the simple sine-Gordon equation. If the spatial coordinate is viewed as a fictitious time, then its form is identical to the equation of motion of a pendulum in a gravitational field. The soliton then corresponds to the following situation. At time $t=-\infty$, place the pendulum in its unstable equilibrium position, pointing upward, opposite to the gravitational field. Give it an infinitesimal kinetic energy δ. It will then swing through 360°, and as $\delta\rightarrow 0$, it will return to its original position at time $t=+\infty$. This orbit, which has zero energy, with energy zero chosen when the pendulum is at rest in the unstable equilibrium position, becomes the sine-Gordon soliton when the time is replaced by the spatial coordinate.

Now give the pendulum a small, but finite amount of kinetic energy ΔE at time $t=-\infty$ (we mean small compared to the gravitational potential energy 2 Mg h). The pendulum will slowly begin to fall, move rapidly past its lower-most point with velocity 2 $(g\,h)^{1/2}$, and return to the topmost point, dwell in its vicinity for some time, and then recycle. We obtain an infinite number of equally spaced "solitons," by virtue of the very small, but finite value of ΔE.

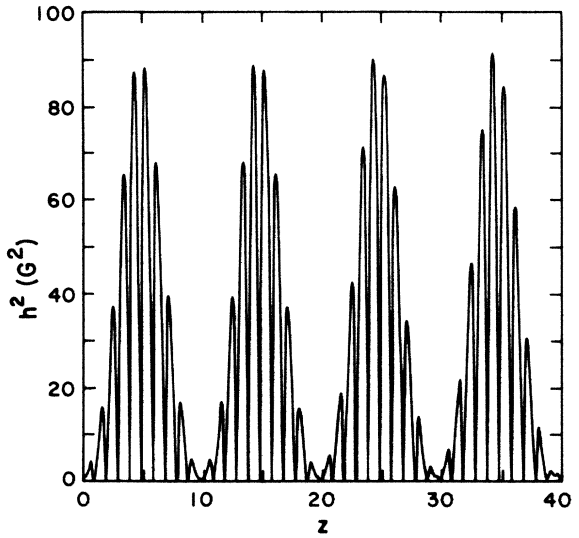

FIG. 8. The field configuration for a 40-bilayer slab, at the first gap-soliton resonance. The bilayer unit used to generate the structure is identical to that employed in Fig. 6. Distance units are the same as in Fig. 7.

The time average of the Poynting vector $\langle S\rangle$ in our problem plays the role of ΔE in the example just given, and we have the time variable replaced by a spatial coordinate. Our "soliton trains" occur only because $\langle S\rangle\neq 0$ when the superlattice is illuminated by incident radiation. Each solitonlike object is not, strictly speaking, a soliton in the mathematical sense, but becomes very similar when the peak field intensity in the medium becomes large compared to that in the incident wave. In Fig. 7(a), the peak field intensity is roughly 2 orders of magnitude larger than the incident field intensity.

We conclude by comparing the field strengths required to enter the highly unstable region when the sample is illuminated with radiation inside an allowed band of linear theory, and the field strengths required to induce gap-soliton-mediated bistability. In Fig. 5(a), the shoulder which separates the regime where $|T|^2$ varies smoothly with $h_i|T|$ from the regime where we have rapid oscillations is $h_i|T|\sim 0.6$, with h_i measured in G. Hence, for this example, incident fields in the range $0.5\leq h_i\leq 1$ G will suffice. Such fields can be attained in contemporary high-power sources. For our example of soliton mediated bistability, we have $h_i\cong 0.1$ G for the first resonance in Fig. 6. Hence, these examples show that the fields required are the same order of magnitude to realize each type of behavior, though for the explicit cases examined, the soliton-mediated bistability occurs at somewhat lower fields. It is quite clear from the calculations presented here that gap-soliton-mediated bistability occurs in multilayer systems at fields very much lower than bistability in a single film. This may be appreciated by comparing Fig. 1(b) with Fig. 6. In the single film, fields as large as 3 G are required to initiate bistability. This conclusion is in agreement with earlier results.

When examining the quantitative results in this paper, the reader should keep in mind that our description of the nonlinear response of the antiferromagnetic films is approximate, in that it assumes the magnetization generated by the electromagnetic field may be written in the form

$$m=\chi_0^{(1)}h+\chi_0^{(3)}|h|^2h \tag{3.3}$$

with higher-order terms ignored. As yet, we have little concrete experimental evidence in hand on the validity of this approximation in an actual material such as FeF_2. The spirit of this study has been to carry out explicit quantitative calculations for superlattice structures that may possibly be synthesized, but at the same time experimental data on the nonlinear response of the antiferromagnetic films are sparse at present.

ACKNOWLEDGMENTS

This research was supported by the U.S. Army Research Office through Grant No. PO-426620. One of us (N.S.A.) acknowledges the support of Conselho Nacional de Desenvolvimento Científico e Tecnológico (CNPq) of Brazil.

*Permanent address: Department of Physics, University of Rhode Island, Kingston, RI 02881-0817.

†Permanent address: Departamento de Física, Universidade Federal do Rio Grande do Norte, 59 000 Natal, Rio Grande do Norte, Brazil.

[1]R. M. Toussaint, D. W. Hone, V. Jaccarino, and S. M. Rezende, Phys. Rev. B **30**, 3859 (1984).

[2]R. E. Camley and D. L. Mills, Phys. Rev. B **29**, 1695 (1984).

[3]R. E. Camley, Talat S. Rahman, and D. L. Mills, Phys. Rev. B **23**, 1226 (1981).

[4]For a recent experiment and references to earlier work, see B. Hillebrands, P. Baumgart, R. Mock, G. Guntherödt, A. Boufelfel, and C. M. Falco, Phys. Rev. B **34**, 9000 (1987).

[5]C. Kittel, in *Introduction to Solid State Physics* (Wiley, New York, 1976), p. 191.

[6]Wei Chen and D. L. Mills, Phys. Rev. Lett. **58**, 160 (1987).

[7]D. L. Mills and S. E. Trullinger, Phys. Rev. B **36**, 947 (1987).

[8]Wei Chen and D. L. Mills, Phys. Rev. B **36**, 6269 (1987).

[9]Francois Delyon, Yves Emmanuel Levy, and Bernard Souillard, Phys. Rev. Lett. **57**, 2010 (1986).

[10]N. S. Almeida and D. L. Mills, Phys. Rev. B **36**, 2015 (1987).

[11]D. Emin and T. Holstein, Phys. Rev. Lett. **36**, 323 (1976).

[12]The electron wave function must necessarily be localized in the plane parallel to the interface for this to be the case [A. Mauger (private communication)]. It is not clear how this can occur, with coherence maintained between the various films in the structure.

[13]Wei Chen and D. L. Mills, Phys. Rev. B **35**, 524 (1987).

[14]Y. B. Band, in *Optical Bistability II,* edited by C. M. Bowden *et al.* (Plenum, New York, 1984).

[15]J. K. Vassiliou, J. Appl. Phys. **59**, 1125 (1986).